

DEIMOS and MOSFIRE spectroscopy of star-forming galaxies in the AKARI NEP-Deep field

Helen K. Kim¹, Matt Malkan¹, Nagisa Oi², Toshinobu Takagi³,
Denis Burgarella⁴, Véronique Buat⁴, Samir Salim⁵, Chris Pearson⁶
and Hideo Matsuhara⁷

¹Department of Physics and Astronomy, UCLA, Los Angeles, CA 90095-1547, USA
email: hkim@astro.ucla.edu

²Tokyo University of Science, 1-3 Kagurazaka, Shinjuku-ku, Tokyo 162-8601, Japan

³Japan Space Forum, 3-2-1, Kandasurugadai, Chiyoda-ku, Tokyo 101-0062, Japan

⁴Laboratoire d'Astrophysique de Marseille, Aix-Marseille Université,
CNRS, F-13013 Marseille, France

⁵Department of Astronomy, Indiana University, Bloomington, IN 47404, USA

⁶Department of Physical Sciences, The Open University, Milton Keynes, MK7 6AA, UK

⁷Institute of Space and Astronautical Science, Japan Aerospace Exploration Agency,
3-1-1 Yoshinodai, Chuo-ku, Sagamihara, Kanagawa 252-5210, Japan

Abstract. Observing high resolution optical to infrared spectra is crucial to understanding how energy is generated in galaxies. We present follow-up optical Keck-II/DEIMOS and infrared Keck-I/MOSFIRE spectra of ~ 200 galaxies in the AKARI/North Ecliptic Pole Deep survey region at intermediate redshift. From rest-frame optical emission lines, we classify most of our objects as star-forming (53%), with the MIR selection favoring relatively massive galaxies (median $\log M/M_{\odot} \sim 10.3$). In addition, we combine our spectroscopic redshifts with UV to FIR photometry as inputs in order to model SEDs with CIGALE, and we measure the PAH $7.7 \mu\text{m}$ luminosity as an SFR indicator.

Keywords. techniques: spectroscopic, galaxies: evolution, infrared: galaxies

1. Introduction

The AKARI North Ecliptic Pole (NEP) Deep Field is a unique region with continuous $2\text{-}24 \mu\text{m}$ coverage in ~ 0.5 square degrees from the Infrared Camera (IRC), providing crucial mid-infrared data of the dust-obscured universe out to $z \sim 1$ ([Murata et al. 2013](#), [Oi et al. 2014](#)). We present optical to NIR spectroscopic results of ~ 200 galaxies in the NEP-Deep field, combining Keck-I/MOSFIRE J- and Y-band and Keck-II/DEIMOS observations. DEIMOS targets prioritized intermediate redshift ($z \sim 1$) sources with AKARI/IRC photometry and Chandra X-ray sources to include possible (obscured) AGN. MOSFIRE targets prioritized strong emission line galaxies with previous optical spectroscopy and AKARI sources in the range $0.7 < z < 1.1$ in order to measure $\text{H}\alpha/\text{[NII]}$. In addition, we used the Y-band to target $\text{H}\alpha/\text{[NII]}$ sources at $0.5 < z < 0.8$.

2. Source Classification

Most of our DEIMOS galaxies on the BPT classification diagram (Fig. 1, left) lie along the star-forming sequence (53%) with 30% composite, 4% Seyfert, and 13% LINERs. In comparison, the sample of AKARI NEP-Wide galaxies ([Shim et al. 2013](#), median $z \sim 0.24$

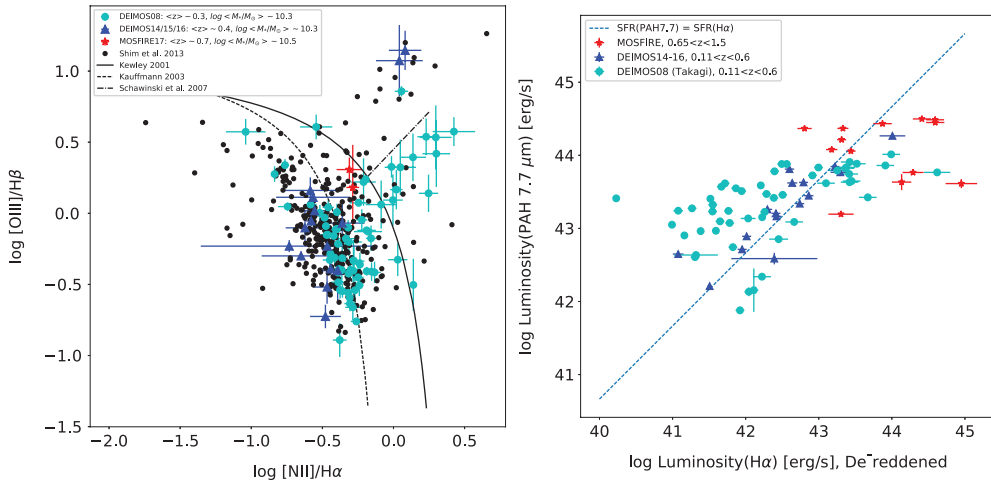


Figure 1. Left: BPT-NII source classification diagram. Right: PAH 7.7 μm luminosity vs. the dust-corrected H α luminosity for combined DEIMOS and (higher z) MOSFIRE sample.

on BPT) contains a smaller fraction of AGN. Our IR-selected sample contains relatively massive galaxies. Although not shown here, the BPT diagram was consistent with the Mass-Excitation Diagram ([OIII]/H β vs. stellar mass).

3. Spectral Energy Distributions and PAH Luminosity Estimates

We combined our spectroscopic redshifts with UV to FIR photometry in order to model SEDs with CIGALE. We assumed a delayed star formation history with exponential burst, Salpeter IMF, and solar metallicity for the stellar model. Key parameters that were allowed to vary included color excess E(B-V) of the young stellar population (0–1.6), mass fraction of PAH dust (0.47–4.58), and AGN fraction (0–0.4).

In order to investigate the PAH 7.7 μm feature as a SF indicator, we compare the PAH 7.7 luminosity from CIGALE best fits to the de-reddened H α luminosity (Fig. 1, right) assuming the Calzetti et al. (2000) extinction law and E(B-V) from CIGALE for our combined DEIMOS S11 ($z \sim 0.5$) and MOSFIRE L15 ($z \sim 1$) sample. The dashed line represents the luminosity relation such that $\text{SFR}(\text{PAH7.7}) = \text{SFR}(\text{H}\alpha)$, where $\text{SFR}(\text{PAH7.7}) [\text{M}_\odot/\text{yr}] = 4.56 \times 10^{-9} \text{ L(PAH7.7)} [\text{L}_\odot]$ (Hernán-Caballero et al. 2009) and $\text{SFR}(\text{H}\alpha) [\text{M}_\odot/\text{yr}] = 5.49 \times 10^{-42} \text{ L(H}\alpha) [\text{erg/s}]$ (Kennicutt et al. 2009). Our limited MOSFIRE points at $z \sim 1$ (red stars) cannot determine how the $\text{SFR}(\text{PAH7.7})/\text{SFR}(\text{H}\alpha)$ correlation evolves from low z to $z > 1$, highlighting the need for further data.

References

- Calzetti, D., Armus, L., Bohlin, R. C., Kinney, A. L., Koornneef, J., & Storchi-Bergmann, T. 2000, *ApJ*, 533, 682
- Hernán-Caballero, A., Pérez-Fournon, I., Hatziminaoglou, E., Afonso-Luis, A., Rowan-Robinson, M., Rigopoulou, D., Farrah, D., Lonsdale, C. J., et al. 2009, *MNRAS*, 395, 1695
- Kennicutt, R. C., Hao, C.-N., Calzetti, D., Moustakas, J., Dale, D. A., Bendo, G., Engelbracht, C. W., Johnson, B. D., et al. 2009, *ApJ*, 703, 1672
- Murata, K., Matsuhara, H., Wada, T., Arimatsu, K., Oi, N., Takagi, T., Oyabu, S., Goto, T., et al. 2013, *A&A*, 559A, 132M
- Oi, N., Matsuhara, H., Murata, K., Goto, T., Wada, T., Takagi, T., Ohyama, Y., Malkan, M., et al. 2014, *A&A*, 566A, 60O
- Shim, H., Im, M., Ko, J., Jeon, Y., Karouzos, M., Kim, S. J., Lee, H. M., Papovich, C., et al. 2013, *ApJS*, 207, 37S